Transmission, Reflection, and Scattering Characterization of Building Materials for Indoor THz Communications

Fatima Taleb, Goretti G. Hernandez-Cardoso, Enrique Castro-Camus, and Martin Koch

***Abstract*—The future communication technologies are naturally evolving toward higher carrier frequencies in order to satisfy the demand for increasing data rates. Terahertz (THz) frequencies appear to make high-speed and high data rate communications possible. However, due to the high free-space damping above 100 GHz, communication systems are limited to short range, seldom, non-line-of-sight transmission links, which rely mostly on the reflection properties of walls and other surfaces. We have investigated the scattering coefficients of a representative collection of 50 building materials used for construction. The optical and reflection properties of the samples were measured using THz time-domain spectroscopy and the scattering coefficients were modeled based on the Fresnel–Rayleigh equations and the Kirchhoff theory. The proposed Kirchhoff–Rayleigh approach is appropriate for the scattering characterization of rough surfaces with limitations to resolve the scattering coefficients of materials with a complex structure. Nonetheless, the measured data show the reflection potential of materials commonly found in indoor environments, giving important insight into the further modeling of THz communication channels.**

***Index Terms*—Building materials, non-line-of-sight (NLOS) transmission links, scattering characterization, terahertz (THz) communications.**

I. Introduction

THE future of high speed, short range, and high data rate communications relies on carrier waves with frequencies above 100 GHz. Many efforts have been made for the development of this technology, for instance, in the early 2000 s, a group led by Tadao Nagatsuma succeeded in transmitting data rates in the range of a few Gb/s at frequencies of 120 GHz [1], later in 2012, Song et al. [2] demonstrated 24 Gb/s data transmission at 300 GHz and most recently, Oshiro et al. [3] introduced the PAM4 modulation for terahertz (THz) wireless communications employing a resonant tunneling diode receiver. THz communications systems, however, are limited by the high free-space damping at frequencies above 100 GHz [4], [5] and many times rely on a line-of-sight link. Nevertheless, a line-of-sight system is likely to be interrupted if objects or people move into the beam path [6], [7]. This problem could be overcome using alternative transmission paths running over indirect non-line-of-sight (NLOS) links [6], [8], [9], including reflections from the walls, as seen in [10, Fig. 1.1] or [6, Fig. 3], along with the ability of steering the beam path. One approach would be microstrip patch antenna arrays. An early design for such antennas for 0.3 THz was reported in [9] and [11]. Another approach is beam-steering devices. Several such devices have been demonstrated [12], [13], [14], [15], [16], [17], yet their capability is still quite limited. In any case, the signal transmission will depend on the reflections from walls and other surfaces; therefore, it is important to know the scattering properties of materials usually found in an interior environment.

To this extent, investigations on the THz and scattering properties of some building materials have been carried out [18], [19], [20], [21]. The reflection properties of only a few selected materials, such as gypsum, plaster, and wallpaper, were studied using THz time-domain spectroscopy and the scattering coefficients were modeled using the Kirchhoff approach [20]. Furthermore, the reflection and scattering properties entered into a ray tracing software to simulate the signal coverage of a typical indoor scenario showing the strong impact of the diffuse scattering on the NLOS propagation paths. This approach and the data presented in [19] and [20] have been used in subsequent years for the design of THz communication systems [22], [23], [24], [25], [26], [27], [28], [29]. Meanwhile, there has been other works demonstrating data transmission over NLOS paths involving the reflection of building materials [5] and the diffuse bistatic scattering response of several metallic rough surfaces [30]. The latter measurements were performed using transmitter and receiver modules operating only at a few frequencies from 100 to 400 GHz.

In this article, we present the investigation of the scattering coefficients of a set of 50 representative building materials commonly found in indoor environments. We studied the optical and reflection properties by means of THz time-domain spectroscopy, characterized the roughness of the surface using photogrammetry and modeled the angle- and frequency-dependent scattering coefficients based on the modified Fresnel equations and an extended Kirchhoff approximation [31]. Finally, we present a detailed discussion for a few exemplary building

Manuscript received 18 November 2022; revised 8 March 2023 and 24 March 2023; accepted 7 April 2023. Date of publication 31 May 2023; date of current version 5 September 2023. This work was supported by the German Research Foundation (DFG) "Meteracom-Metrology for THz Communications" under Grant FOR 2863. The work of Enrique Castro-Camus was supported by Alexander von Humbolt Foundation. *(Corresponding author: Enrique Castro-Camus.)*

The authors are with the Department of Physics, Philipps-Universität Marburg, 35037 Marburg, Germany (e-mail: fatima.taleb@physik.uni-marburg.de; goretti.hernandezcardoso@physik.uni-marburg.de; enrique.castrocamus@physik.uni-marburg.de; martin.koch@physik.uni-marburg.de).

This article has supplementary material provided by the authors and color versions of one or more figures available at https://doi.org/10.1109/TTHZ.2023.3281773.

Digital Object Identifier 10.1109/TTHZ.2023.3281773

TABLE I
BUILDING PRODUCTS LISTED BY MATERIAL TYPE

Material	Sample
Structural	(1x) Fire clay brick (2x) Cement (1x) Concrete (1x) Lime with marble grains (2x) Layered mixture of gypsum and carton (3x) Composite of gypsum and aggregate (1x) Gypsum board
Wood	(3x) Raw wood (3x) Compressed wood (2x) High-density fiberboard (1x) Magnesite-bonded wood
Insulation	(1x) Bitumen balin membrane (1x) Acoustic panel (1x) Mineral insulation board
Ceramic and stone	(6x) Ceramic tiles (3x) Marble
Plastic	(1x) Polyurethane coating (1x) Plexiglass
Glass	(1x) White glass (1x) Dark glass
Caulking compounds	(2x) Silicone (1x) Installation glue (2x) Filling coating (1x) Acrylic (1x) Wood putty (1x) Plaster
Foam	(1x) Spray foam (1x) Laminate pad (1x) Polystyrene
Fabric	(1x) Carpet
Paint	(1x) Colored lacquer (1x) Wall paint

samples regarding the differences between the measured and modeled data to set the limitations that the scattering model is to overcome for the further calculations of indoor THz communication channels.

II. MEASUREMENTS

A representative collection of 50 building materials used for construction was studied. The set of samples covers from naturally occurring materials to man-made products, all commonly present in indoor environments. A complete list of the samples, classified by material type, is presented in Table I.

For a comprehensive understanding of the scattering properties, the diffuse reflection was measured and compared with the modeled scattering coefficients. For this purpose, all materials were prepared into 5 cm $\times$ 5 cm samples, the roughness of the surface was characterized, and the optical properties and the reflection and scattering coefficients were investigated at THz frequencies.

A. Surface Characterization

The roughness profile of the building materials was characterized by means of photogrammetry. Photogrammetry is a technique used to reconstruct an object three-dimensionally by combining many photographic images. The object is photographed from different angles and a 3-D model is created combining the information contained in the photographs of the object, from which physical characteristics are calculated. Using this technique, every sample was placed on a rotational stage and 50 photographs were acquired using a professional digital camera, the 3-D model reconstruction was performed using the free version of the 3DF Zephyr software, and the roughness profile of the material surface was calculated with the open-source and free software CloudCompare. From the 3-D model, further calculations, such as the standard deviation σ of the surface height distribution and the correlation length L, which indicates the correlation between the heights of adjacent points, were performed as described in [20]. An example of the roughness characterization of a sample can be seen in Fig. 1.

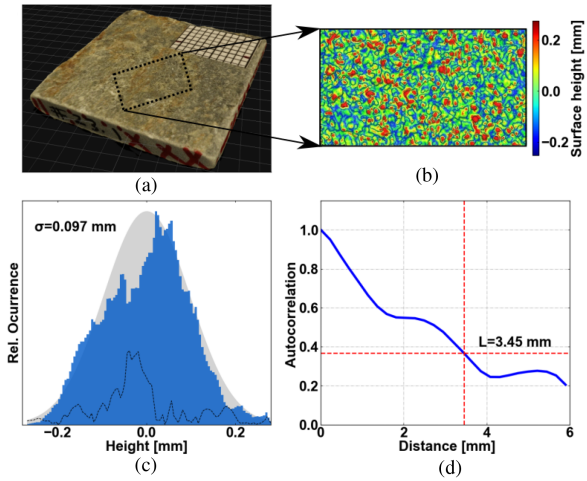

Fig. 1. Surface characterization of a building material. The sample is (a) three-dimensional modeled by means of photogrammetry then, the (b) surface heights are calculated from which the (c) height distribution and (d) correlation length are determined.

B. Optical Properties and Reflection Characterization

The transmission, reflection, and scattering properties of the building materials for TM polarization were investigated by means of a terahertz time-domain spectrometer (THz-TDS), as schematically depicted in Fig. 2. The optical properties were studied with the THz-TDS system in transmission configuration. Reference waveforms were recorded in the absence of sample, and subsequently, samples were placed in the THz beam path. The waveforms acquired were preprocessed by removing the dc offset they had and were windowed in order to remove spurious echoes in the signal coming either from reflections in the TDS system or the sample itself. The refractive index was determined following the methodology described in [32], which in brief leads to the following equations:

$$n(\omega) = 1 - \frac{c}{\omega l}(\phi_{\text{sample}} - \phi_{\text{reference}}) \tag{1}$$

and

$$\kappa(\omega) = -\frac{c}{\omega l}\ln\left(\frac{(n(\omega)+1)^2}{4n(\omega)}\frac{|E_{\text{sample}}|}{|E_{\text{reference}}|}\right) \tag{2}$$

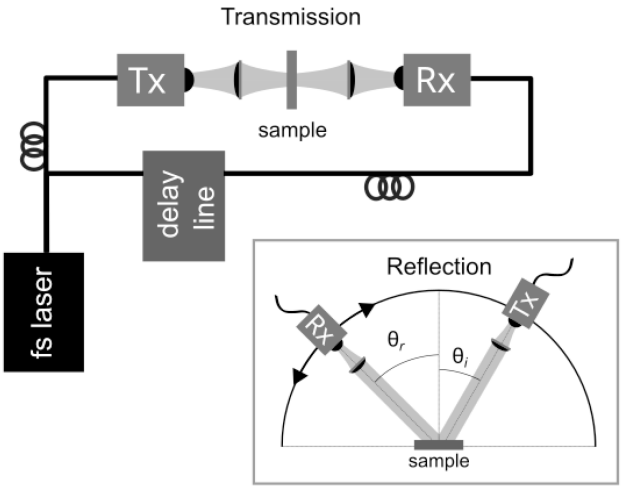

Fig. 2. THz-TDS. In transmission configuration, the emitter (Tx) and receiver (Rx) are facing each other, a pair of lenses drive the THz radiation from the emitter through the sample and to the receiver in a single optical axis. In the inset, the THz-TDS spectrometer is mounted on a goniometer system in reflection geometry. The emitter (Tx) and receiver (Rx) are placed at a certain angle from each other facing two optical axes.

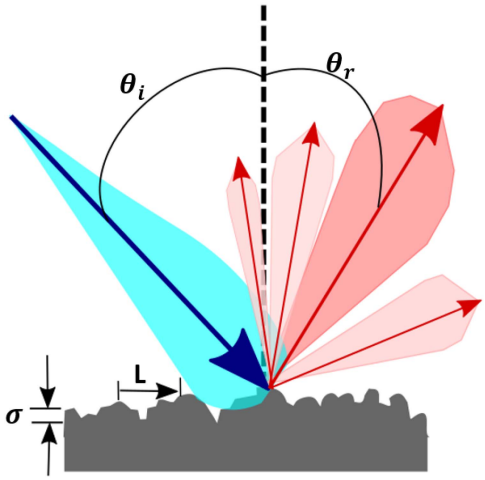

Fig. 3. Scattering from a rough surface with height distribution σ and autocorrelation length L. The incident wave under the angle θ_i is reflected in the direction of θ_r.

where ϕ_i and $|E_i|$ are the phase and amplitude of the Fourier transforms for $i =$ sample/reference, c is the speed of light, ω is the angular frequency, and l is the thickness of the sample, which was determined by using a digital vernier. The thicknesses, refractive indices, and extinction coefficients of all samples are provided in the supplementary material. The reflectivity of the sample was then calculated by means of the Fresnel coefficient r_{TM}. Subsequently, the emitter and receiver antennas of the spectrometer were placed on the arms of a goniometer system (inset to Fig. 2) and the THz signal scattered from the sample was recorded at different angles fixing the position of the THz emitter at $\theta_i = 30^\circ$, while the THz receiver was swept over the angle range from $\theta_r = 0^\circ$ to $\theta_r = 90^\circ$ with 1° step. Likewise, reference waveforms were recorded replacing the sample by a metal plate. The illuminated area was approximately 4 cm^2.

The THz-TDS system we used is based on an Er:fiber laser, which produces ~90 fs pulses at a repetition rate of 100 MHz, with an average power of ~120 mW and central wavelength of 1550 nm. The pulses were split into two parts: the first one was fiber coupled and sent to a biased InGaAs photoconductive emitter in order to produce THz transients, while the second part of the pulse was sent to a computer-controlled delay line, and subsequently, fiber coupled and sent onto an InGaAs photoconductive detector. By recording the current in the photoconductive detector as a function of the delay-line position, it is possible to reconstruct the time-dependent waveform of the THz electromagnetic transient.

C. Kirchhoff–Rayleigh Scattering Model

The proper modeling of the scattering patterns of indoor building materials strongly depends on the geometry of their surfaces. For instance, the reflection properties of smooth, optically thick materials, in which specular reflection dominates, can be easily characterized with the Fresnel equations [18]. Yet, most of the building materials have rather rough surfaces and diffuse reflections need to be considered. To this extend, the Kirchhoff theory of scattering from rough surfaces can be implemented to model the losses in the specular direction and the diffuse reflection patterns.

In this study, we characterize the scattering patterns of a wide set of materials, with surfaces ranging from smooth ($\sigma = 0.009$ mm) to rough ($\sigma = 0.5$ mm) by means of the Rayleigh-modified Fresnel equations and the extended Kirchhoff theory merged together in what we refer as the Kirchhoff–Rayleigh model. Each approach is weighted by an error function centered at λ_0, threshold wavelength at which the surface is considered smooth, calculated from the Fraunhofer criterion [33]

$$\sigma = \frac{\lambda_0}{32\cos\theta_i} \tag{3}$$

where θ_i is the incident angle with respect to the normal of the surface and σ is the standard deviation of the surface height distribution (see Fig. 3).

Therefore, depending on the roughness of the surface, the specular reflection and diffuse scattering patterns are calculated following the Fresnel equations modified with the Rayleigh roughness factor or the extended Kirchhoff theory, on a weighted contribution of both, the main formulations of which are described in the following.

1) Specular Reflection, the Rayleigh–Fresnel Equations: When a plane wave is reflected from a smooth surface, the reflectivity in the specular direction can be calculated using the simple Fresnel reflection coefficients. In reality, however, surfaces are mostly found to be rough and the reflection power is reduced due to diffuse scattering. Hence, in order to fully describe the reflectivity in the specular direction for the case of a smooth to moderately rough ($\sigma < \lambda_0/32\cos\theta_i$) surface, the Fresnel reflection coefficients are multiplied by the Rayleigh roughness factor [18]

$$\rho = e^{-g/2} \tag{4}$$

where

$$g = \left(\frac{4\pi\sigma\cos\theta_i}{\lambda_i}\right)^2 \tag{5}$$

with θ_i being the incident angle, σ the standard deviation of the surface roughness, and λ_i the free-space wavelength of the incident wave. Then, the modified reflection coefficient r'_{TM} is given by

$$r'_{\mathrm{TM}} = \rho \cdot r_{\mathrm{TM}} \tag{6}$$

where r_{TM} is the Fresnel reflection coefficient for TM-polarized waves incident on a smooth surface, which can be calculated from the frequency-dependent refraction index n.

It has to be noted that this approximation does not provide an angular-dependent function that describes how the radiation lost in the specular direction is redirected in other directions. Yet, if the wavelength is long in terms of the Fraunhofer criterion (3), the loss would be $\leq 1.5\%$ at an incidence angle of 30°. Therefore, to first approximate, the only measurable effect is the loss in the specular reflection, and we have, thus, assumed that the nonspecular components are negligible in the Fraunhofer regime.

2) Diffuse Scattering, the Extended Kirchhoff Theory: The modified Fresnel coefficient describes the reflectivity in the specular direction accounting for the losses due to diffuse scattering. Furthermore, the diffuse reflections for rougher surfaces can be described by an extended model of the Kirchhoff theory, previously proposed to investigate the scattering properties of typical indoor building materials [20], which states that a wave incident on an optically thick, rough surface under an angle θ_i is scattered in the direction given by the angle θ_r (as in Fig. 3) as follows:

$$\langle\rho\rho^*\rangle = \langle rr^*\rangle \cdot \langle\rho\rho^*\rangle_\infty \tag{7}$$

where r, given by $r_{\mathrm{TM}} = (\cos\theta_i - n)/(\cos\theta_i + n)$, denotes the Fresnel reflection coefficient of the scattering surface and $\langle\rho\rho^*\rangle_\infty$ describes the mean scattering coefficient of an infinitely conductive surface as

$$\langle\rho\rho^*\rangle_\infty = e^{-g} \cdot \left(\rho_0^2 + \frac{\pi L^2 F^2}{A}\sum_{m=1}^{\infty}\frac{g^m}{m!m}e^{-(v_x^2+v_y^2)L^2/4m}\right) \tag{8}$$

with

$$\rho_0 = \mathrm{sinc}(v_x l_x) \cdot \mathrm{sinc}(v_y l_y) \tag{9}$$

$$v_x = k \cdot (\sin\theta_i - \sin\theta_r) \tag{10}$$

$$v_y = k \cdot (-\sin\theta_r) \tag{11}$$

$$g = k^2\sigma^2(\cos\theta_i + \cos\theta_r)^2 \tag{12}$$

and

$$F(\theta_i, \theta_r) = \frac{1 + \cos\theta_i\cos\theta_r - \sin\theta_i\sin\theta_r}{\cos\theta_i(\cos\theta_i + \cos\theta_r)}. \tag{13}$$

Here, $A = l_x \cdot l_y$ is the illuminated area, k represents the free-space wavenumber, and the Rayleigh roughness factor g, given by (12), is an indicator of the relative surface roughness at a given wavelength.

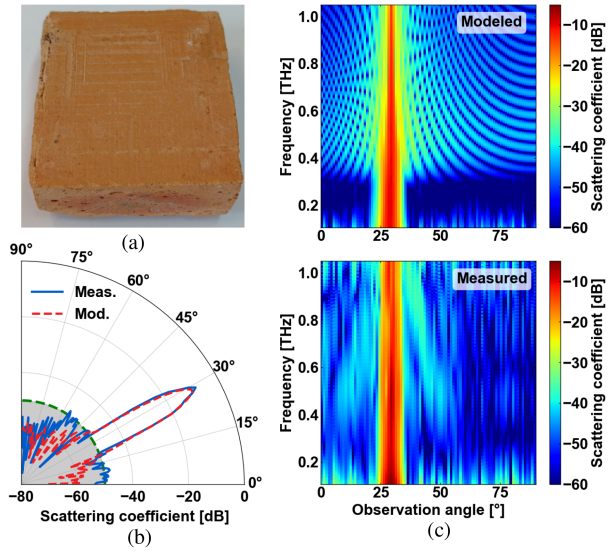

Fig. 4. (a) Photograph of a fire clay brick sample. (b) Measured and modeled scattering coefficients at 300 GHz as a function of the reflected angle, the green line shows the noise level of the THz-TDS system. (c) Color map of the modeled and measured scattering coefficients as a function of frequency and reflected angle.

Finally, the scattering coefficients are calculated as function of the frequency f by

$$s(f) = \mathrm{erf}\left(\frac{\lambda - \lambda_0}{\sigma_{\mathrm{err}}}\right) \cdot \langle\rho\rho^*\rangle + \left[1 - \mathrm{erf}\left(\frac{\lambda - \lambda_0}{\sigma_{\mathrm{err}}}\right)\right] \cdot r'_{\mathrm{TM}} r'^*_{\mathrm{TM}} \tag{14}$$

valid for a wavelength range λ, with λ_0 given by the Fraunhofer criterion in (3), and a standard deviation σ_{err}. The reflection coefficients according to the extended Kirchhoff theory $\langle\rho\rho^*\rangle$ and the Rayleigh–Fresnel equation r'_{TM} are given by (6) and (7), respectively.

III. Results

The scattering coefficients of the investigated building materials have been found to vary significantly depending not only on the optical properties and roughness of the surface but also on the material composition and its internal structure. In the following, we present a few examples of the scattering characterization of some structural materials, insulators, caulking compounds, and other building products. The scattering characterization of all building materials is found in the supplementary material, and the corresponding figures are referred with the prefix S.

Starting with structural materials, we studied bricks, stone, cement, and different gypsum and wood samples. A photograph of a fire clay brick, with a slightly rough surface (σ = 0.024 mm), is shown in Fig. 4(a) together with a polar plot of the scattering coefficient at 300 GHz as a function of the reflected angle in Fig. 4(b). We picked 300 GHz since it is one of the target frequencies for the next generation of telecommunication systems; however, the measured and calculated frequency and angle-dependent scattering coefficient between 0.1 THz and 1.0 are shown as color maps in Fig. 4(c). The lobe in the specular direction is nicely resolved, showing a good agreement between

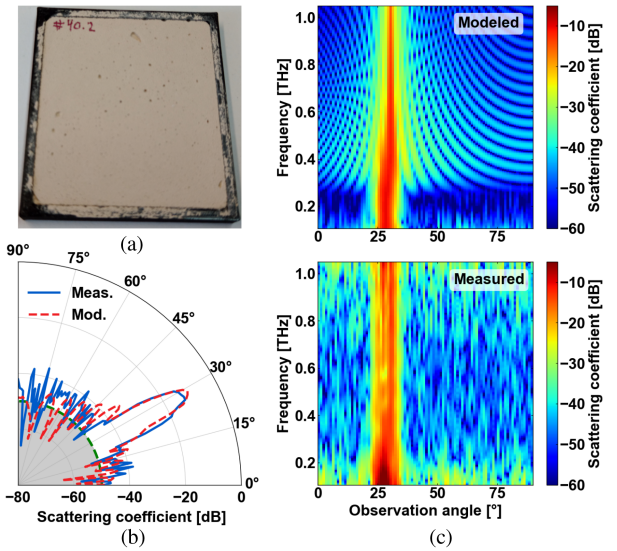

Fig. 5. (a) Photograph of a Flexfuge cement sample. (b) Measured and modeled scattering coefficients at 300 GHz as a function of the reflected angle, the green line shows the noise level of the THz-TDS system. (c) Color map of the modeled and measured scattering coefficients as a function of frequency and reflected angle.

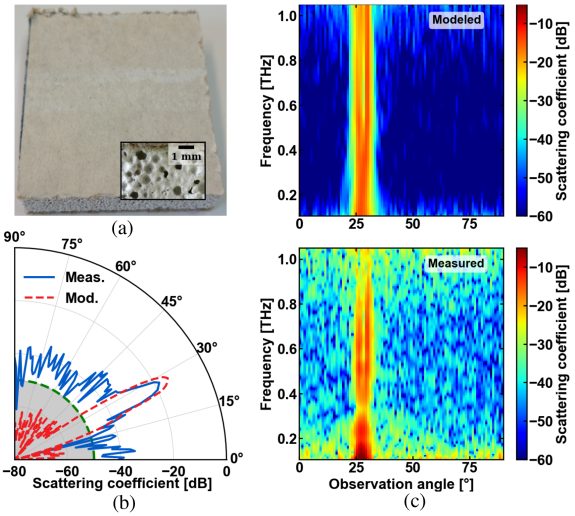

Fig. 6. (a) Photograph of a gypsum–carton layered sample, the inset shows a microscopic image of its longitudinal section. (b) Measured and modeled scattering coefficients at 300 GHz as a function of the reflected angle, the green line shows the noise level of the THz-TDS system. (c) Color map of the modeled and measured scattering coefficients as a function of frequency and reflected angle.

measurements and modeling, with sidelobes in the nonspecular direction falling below the noise threshold.

Two different types of cement, Flexfuge and Universal, a Beton concrete sample, and lime with marble grains were also analyzed. The scattering characterization of a sample of Flexfuge cement with $\sigma = 0.029$ mm can be seen in Fig. 5. The scattering coefficient at 300 GHz as a function of the reflected angle in Fig. 5(b) shows a well-resolved lobe in the specular direction with sidelobes right above the noise level. This good agreement between the modeled and measured data is also observed on the frequency- and angle-dependent scattering coefficients in Fig. 5(c). Moreover, we could see a similar behavior on the Universal cement sample (see Fig. S3) and on the Beton concrete (see Fig. S4). These materials are particularly interesting since they are usually left unfinished after being cast. On one hand, their nice reflection properties are not influenced by covering materials and, on the other hand, diffuse scattering could follow the patterns imprinted on the surface by the formwork. This response could be seen in the sample of lime with marble grains (see Fig. S5) with a good reflection coefficient in the specular direction and nice diffuse scattering patterns given by the marbles on the surface.

As for gypsum materials, we investigated composites, either mixed or layered, of gypsum and different aggregates. The scattering characterization of a gypsum–carton layered sample is shown in Fig. 6 as an example. As seen in the photograph of Fig. 6(a), the sample has a smooth surface with $\sigma = 0.009$ mm and a porous internal structure, noticeable on the inset. This particular composition of the sample could explain how the modeled and measured scattering coefficients roughly correlate in the scattering coefficient at 300 GHz as a function of the reflected angle, as shown in Fig. 6(b), and in the frequency-dependent scattering patterns, as shown in Fig. 6(c). The lobe measured in the specular direction is barely resolved with even larger differences between the measured and modeled data of the nonspecular lobes. We believe that the top thin layer on the sample together with its porous structure may lead to multiple internal reflections that could contribute to the measured diffuse scattering. A similar behavior with better agreement between the modeled and measured data was observed in a second gypsum–carton layered sample (see Fig. S7). A reasonable good scattering response of the mixtures of gypsum and different aggregates (see Fig. S8–Fig. S10) was observed only with slight variations depending on the reflection properties of the aggregates; meanwhile, the scattering coefficients of a gypsum sample with a rough surface and high porosity could merely be resolved above the noise level (see Fig. S11).

Different samples of wood-based materials, ranging from raw to compressed wood, were studied. In Fig. 7, the scattering characterization of a raw wood sample, namely Spruce Fir, is presented. The surface is considered to be nearly smooth ($\sigma = 0.014$ mm) with a fibrous structural tissue, as seen in Fig. 7(a). A slight agreement between the modeled and measured diffuse scattering can be observed in the scattering coefficient at 300 GHz as a function of the reflected angle, as shown in Fig. 7(b), and in the frequency-dependent scattering patterns, as shown in Fig. 7(c). The measured lobe in the specular direction is nearly resolved with a small difference in the amplitude. The nonspecular lobes, on the contrary, are barely seen in the theoretical curve, whereas a multitude is measured in the experiments with notable differences in amplitude. This inconsistency between modeling and measurements could be attributed to the fibrous structure of the raw wood contributing to multiple internal reflections. The same behavior was observed on a second sample of Spruce Fir (see Fig. S13) and on a sample of Douglas Fir wood (see Fig. S14).

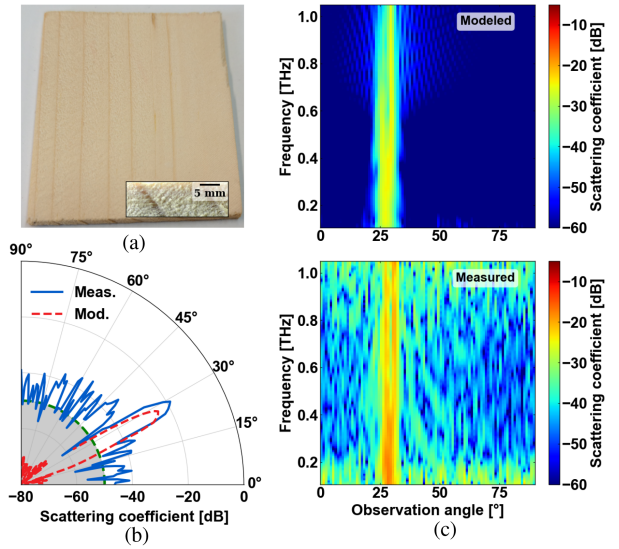

Fig. 7. (a) Photograph of a Spruce Fir wood sample, the inset shows a microscopic image of its longitudinal section. (b) Measured and modeled scattering coefficients at 300 GHz as a function of the reflected angle, the green line shows the noise level of the THz-TDS system. (c) Color map of the modeled and measured scattering coefficients as a function of frequency and reflected angle.

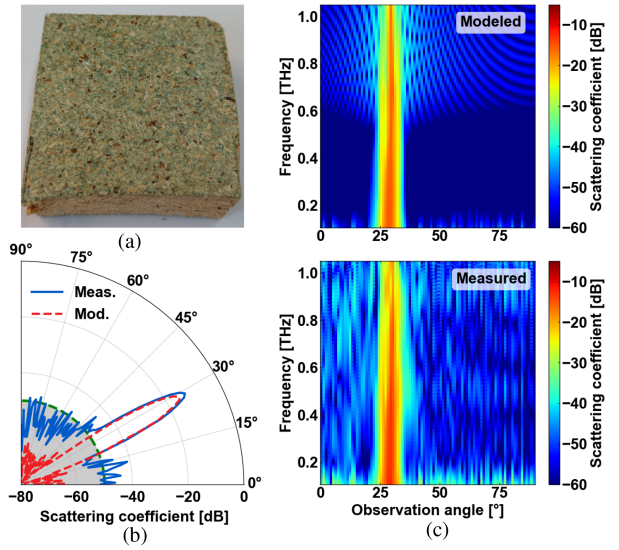

Fig. 8. (a) Photograph of a compressed wood sample. (b) Measured and modeled scattering coefficients at 300 GHz as a function of the reflected angle, the green line shows the noise level of the THz-TDS system. (c) Color map of the modeled and measured scattering coefficients as a function of frequency and reflected angle.

In addition, the characterization of a compressed wood sample with a nearly smooth surface ($\sigma = 0.014$ mm) is shown in Fig. 8. Compared with the porous raw wood, there is a better agreement between the modeled and measured scattering coefficients with a well-resolved specular lobe in both, the scattering coefficient at 300 GHz as a function of the reflected angle and the scattering patterns as a function of the frequency, see Fig. 8(b) and (c), respectively. Multiple lobes in the nonspecular direction are present in the modeling that fall below the noise level. Contrary to the raw wood, the compression of the wood fibers in this sample reduces the air gaps in the internal structure, which results in a higher refractive index and in a larger reflectivity. Two other samples of compressed wood (see Figs. S16 and S17) and two more of high-density fiberboard (see Figs. S18 and S19) present similar reflection patterns, with a nicely resolved lobe in the specular direction and the diffuse scattering coefficients depending only on the roughness of their surfaces.

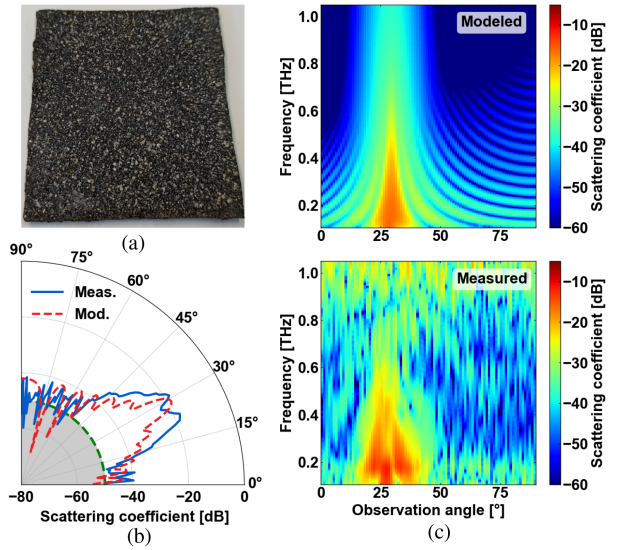

Fig. 9. (a) Photograph of a Bitumen Balin membrane. (b) Measured and modeled scattering coefficients at 300 GHz as a function of the reflected angle, the green line shows the noise level of the THz-TDS system. (c) Color map of the modeled and measured scattering coefficients as a function of frequency and reflected angle.

Other interesting building products are insulators. Although insulators are mostly underneath the surface coating, in some cases, these materials are used as false ceilings or as wall coverings. In this work, we investigated different insulation materials. In Fig. 9, the scattering characterization of a Bitumen Balin membrane can be seen. Bitumen, also known as asphalt, is a composition of many mineral materials with different particle sizes, which makes the membrane surface rough ($\sigma = 0.087$ mm). The scattering coefficient at 300 GHz as a function of the reflected angle in Fig. 9(b), and the angle- and frequency-dependent scattering coefficients in Fig. 9(c) show a reasonable agreement between the measured and modeled data with a broad lobe in the specular direction and the nonspecular patterns well resolved even with similar amplitudes right above the noise level. At higher frequencies, however, this agreement is not longer observed due to the increasing noise impact given by the high-frequency roll-off of the signal-to-noise ratio of the THz-TDS system. A multilayered acoustic panel (see Fig. S22) with a smooth surface and air gaps within the structure was also studied showing a similar response as the Bitumen membrane only with a slight difference in the amplitude of the main lobe, probably due to the contribution of air on the reflection coefficient. Different is the case for a mineral insulation board (see Fig. S23) with a rough surface and a highly porous structure, which results in scattering coefficients falling below the noise level.

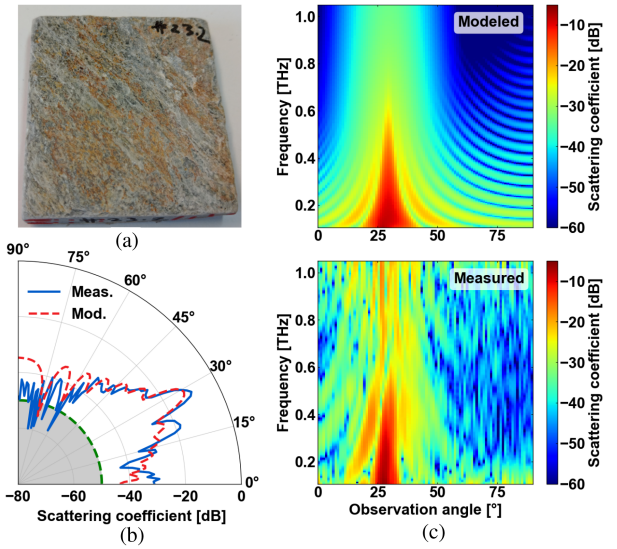

Fig. 10. (a) Photograph of a ceramic tile with a rough surface. (b) Measured and modeled scattering coefficients at 300 GHz as a function of the reflected angle, the green line shows the noise level of the THz-TDS system. (c) Color map of the modeled and measured scattering coefficients as a function of frequency and reflected angle.

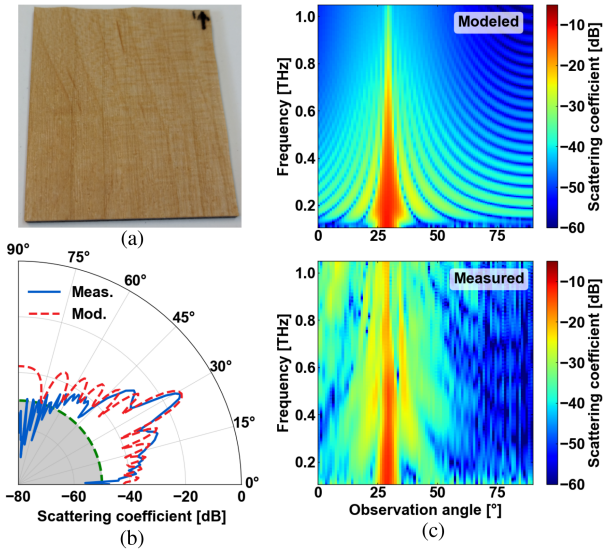

Fig. 11. (a) Photograph of a tile with a polyurethane coating. (b) Measured and modeled scattering coefficients at 300 GHz as a function of the reflected angle, the green line shows the noise level of the THz-TDS system. (c) Color map of the modeled and measured scattering coefficients as a function of frequency and reflected angle.

Multiple samples of plastic, glass, ceramic, and marble were analyzed too. These materials are commonly found in indoor environments as floor tiles, wall coverings, room dividers, and decoration. Therefore, a comprehensive knowledge of their scattering patterns is of special interest for the indoor communication channels. Examples of the scattering characterization of these materials are presented in the following paragraphs. The scattering coefficients of a ceramic tile is shown in Fig. 10. A good agreement can be observed in the scattering coefficient at 300 GHz as a function of the reflected angle in Fig. 10(b), with a nicely resolved lobe in the specular direction and the sidelobes reasonably following the modeled patterns. The measured and simulated scattering coefficients as a function of both, frequency and the observation angle, are presented in Fig. 10(c). The main and surrounding lobes are comparable with the modeled data; nevertheless, as the observation angle falls off the specular direction, the noise impacts the data quality due to the much lower signal levels. Same is the case for higher frequencies. Yet, and despite the rough surface of the ceramic tile with $\sigma =$ 0.097 mm, the overall scattering behavior is well modeled.

Some indoor tiles have a thin plastic coating to produce a wood-like finishing. These plastic coatings are similar to ceramics in terms of structure, such as roughness and surface regularity, and the optical properties, i.e., refractive index and reflectivity. The scattering characterization of a tile with a polyurethane coating is seen in Fig. 11. A similar behavior to the ceramic tile can be observed on the scattering coefficient at 300 GHz as a function of the reflected angle in Fig. 11(b), and on the scattering coefficients as a function of the frequency and observation angle in Fig. 11(c). The main lobe is nicely resolved along with the sidelobes, except those far away the specular direction, which are likely buried in noise. This nice agreement between modeling and measurements was also observed in all the ceramic and

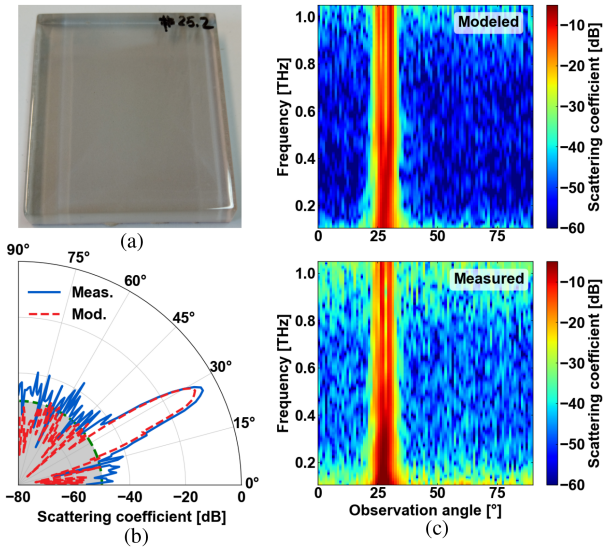

Fig. 12. (a) Photograph of a white glass sample. (b) Measured and modeled scattering coefficients at 300 GHz as a function of the reflected angle, the green line shows the noise level of the THz-TDS system. (c) Color map of the modeled and measured scattering coefficients as a function of frequency and reflected angle.

marble tiles (see Figs. S25–S32), as well as in the plexiglass sample (see Fig. S34), each with a wel-resolved main lobe in the specular direction and sidelobes right above the noise level.

Another interesting material for this study is glass, particularly due to its larger refractive index at THz frequencies that results in a higher reflectivity than for other materials found indoors. The scattering characterization of a smooth sample of glass with $\sigma = 0.009$ mm is presented in Fig. 12. The scattering coefficient at 300 GHz as a function of the reflected angle in Fig. 12(b), along with the scattering coefficients as a function of

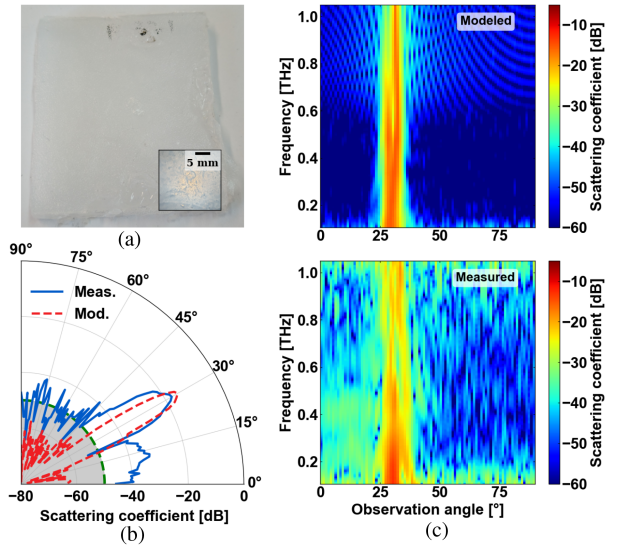

Fig. 13. (a) Photograph of a silicone sample, the inset shows a microscopic image of the surface. (b) Measured and modeled scattering coefficients at 300 GHz as a function of the reflected angle, the green line shows the noise level of the THz-TDS system. (c) Color map of the modeled and measured scattering coefficients as a function of frequency and reflected angle.

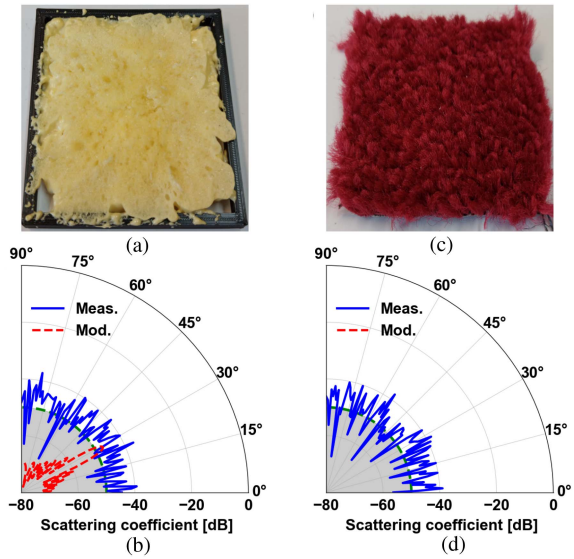

Fig. 14. Photograph of (a) spray foam and (c) carpet. Correspondent measured and modeled scattering coefficients at 300 GHz as a function of the reflected angle. The modeled coefficients in (d) fall below −80 dB. The green line shows the noise level of the THz-TDS system.

both, the frequency and the observation angle in Fig. 12(c), show a very good agreement between the measured and the modeled data and are mainly determined by the reflection in the specular direction. The same response in the scattering coefficients of the dark glass (see Fig. S36) was observed.

Moreover, we investigated the so-called caulking compounds, flexible sealing materials used to close up gaps in building structures. As an example, the scattering characterization of a silicone sample is shown in Fig. 13. Surprisingly, and despite silicone exhibits a relatively small refractive index in the THz range, its modeled and measured scattering coefficients at 300 GHz as a function of the observation angle in Fig. 13(b) and as a function of the angle and frequency in Fig. 13(c) show a reasonable agreement with a well-resolved lobe in the specular direction. Yet, the measured data in the nonspecular direction do not agree as nicely to the modeled data, possibly due to air bubbles in the silicone sample, visible in the inset, which could cause internal reflections contributing to a stronger diffuse scattering, and the varying thickness along the surface sample, which leads to unexpected nonspecular lobes. A similar behavior could be seen in the second sample of silicone (see Fig. S38) and, overall, in all the caulking materials (see Fig. S39–S44) studied in this work, probably due to their flexible nature and application technique.

The reflection properties of other building products, such as paint, textiles, and foam materials, were also studied. For example, the scattering characterization at 300 GHz of spray foam and of a piece of carpet can be observed in Fig. 14. As for the spray foam sample in Fig. 14(a) with $\sigma = 0.1$ mm, the modeled scattering coefficient at 300 GHz as a function of the observation angle in Fig. 14(b) shows a main lobe in the specular direction with decreasing sidelobes. Nevertheless, the modeled data fall below the noise level of our measurement system and, therefore, the measurements cannot resolve the scattering patterns. We could observe the same behavior in two more foam samples, namely a laminate pad (see Fig. S46) and polystyrene foam (see Fig. S47). Foam materials exhibit a refractive index of approximately 1 at THz frequencies, resulting in a reflection coefficient close to zero, hence the low scattering coefficients. Similar is the case for the piece of carpet in Fig. 14(c) with a refractive index of 1.05, a surface considered as highly rough with $\sigma = 0.5$ mm and a significantly fibrous structure, resulting all together in scattering coefficients falling far below −80 dB and, therefore, not depicted in Fig. 14(d), where we can see the measured data right at the noise level. Contrary to foam and fabric materials, the colored lacquer (see Fig. S49) and wall paint (see Fig. S50) samples exhibit better reflection properties with a reasonable well-resolved lobe in the specular direction and nice diffuse scattering patterns. However, defects in the paint layers, such as cracking, flaking, and clumping, should be considered as they may lead to different scattering coefficients.

It can be noticed that the traditional scattering theories, on which the Kirchhoff–Rayleigh model used in this study is based, have certain limitations. For instance, the Kirchhoff approximation fails if the surface has sharp edges, spikes, or other geometrical irregularities sometimes encountered in some indoor building materials. Moreover, multilayered and/or porous structures are not considered in the scattering model, which may lead to multiple internal reflections and interfacial scattering, that contribute to the experimentally measured behavior. A very clear example of these limitations is observed in the scattering characterization of a magnesite-bonded wood sample with a highly rough surface ($\sigma = 0.27$ mm) and a multilayered carton structure, as shown in Fig. 15. As observed in Fig. 15(b) and 15(c), a single lobe in the specular direction is modeled. However, the measured data show not only the main lobe in

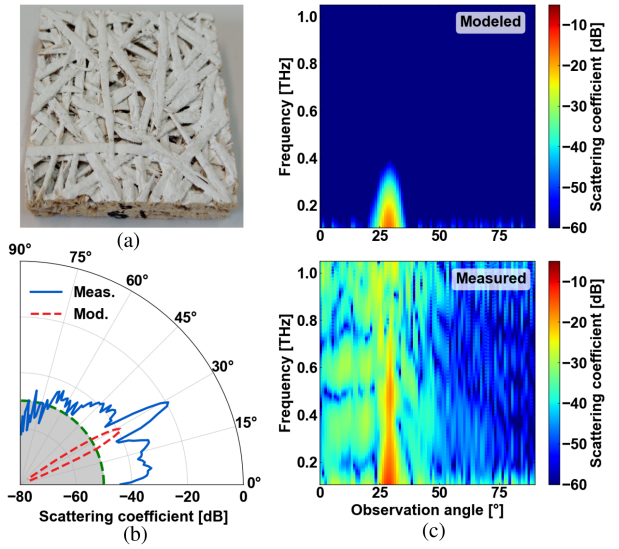

Fig. 15. (a) Photograph of a magnesite-bonded wood sample. (b) Measured and modeled scattering coefficients at 300 GHz as a function of the reflected angle, the green line shows the noise level of the THz-TDS system. (c) Color map of the modeled and measured scattering coefficients as a function of frequency and reflected angle.

the specular direction but also strong diffuse scattering with amplitudes above the noise level. This disagreement between the modeled and measured scattering coefficients could be attributed to the complex composition of the sample with several layers of wood fibers randomly bonded together and a very irregular surface with multiple sharp edges and air gaps, as seen in Fig. 15(a). None of these features are considered by the traditional scattering models and highlight the limitations of the Kirchhoff–Rayleigh approach for the modeling of the reflection properties of indoor building materials. Therefore, improvements on the model remain to be made for the further modeling of indirect THz communication channels.

IV. Conclusion

We have presented the investigation of the scattering coefficients of a representative collection of 50 building materials. The optical and reflection properties of all samples were measured using a fiber-coupled THz-TDS, the roughness characterization was performed by means of photogrammetry, and the specular reflection and diffuse scattering coefficients were modeled based on the modified Fresnel equations and the extended Kirchhoff theory. The measured refractive indices and scattering coefficients show promising reflection properties of some materials commonly found in indoor environments, e.g., glass, ceramic, stone, plastic, and cement composites. Other materials, such as foam, textiles, and porous compounds, exhibit rather low reflectivity, yet these building products are usually encountered underneath a covering surface. Comparing measured with modeled data, the proposed Kirchhoff–Rayleigh approach is shown to be appropriate for the scattering characterization of building materials with random rough surfaces. However, the model fails to reproduce the scattering behavior of samples with a complex structure. Materials with complex structures have particular features, such as sharp edges, air gaps, and other geometrical irregularities on the surface, and a multilayered and/or porous bulk structure, which either violate some assumptions of the Kirchhoff theory or are not considered in any of the traditional scattering approximations. That is the case for multilayered and porous structures, which lead to multiple internal reflections, that contribute to the scattering properties of the material. Yet, and despite these features are not considered for the modeling of the scattering coefficients in this study, the measured data offer valuable insights into the scattering potential of these rough and multilayered materials commonly found in indoor environments, making the NLOS THz data transmission a more real case scenario. This contribution is the first comprehensive study on the optical behavior of broad families of building materials and is expected to be very relevant for the future design of THz frequency communication systems. Modifications in the scattering Kirchhoff–Rayleigh approximation for the proper modeling of THz communication channels are left for future works.

Data Availability

The surface, transmission, reflection, and scattering characterization data are available on https://doi.org/10.6084/m9.figshare.21539109.

References

[1] A. Hirata, M. Harada, and T. Nagatsuma, "120-GHz wireless link using photonic techniques for generation, modulation, and emission of millimeter-wave signals," *J. Lightw. Technol.*, vol. 21, no. 10, pp. 2145–2153, Oct. 2003.

[2] H.-J. Song et al., "24 Gbit/s data transmission in 300 GHz band for future terahertz communications," *Electron. Lett.*, vol. 48, no. 15, pp. 953–954, 2012.

[3] A. Oshiro et al., "PAM4 48-Gbit/s wireless communication using a resonant tunneling diode in the 300-GHz band," *IEICE Electron. Express*, vol. 19, no. 2, 2021, Art. no. 20210494.

[4] R. Piesiewicz et al., "Short-range ultra-broadband terahertz communications: Concepts and perspectives," *IEEE Antennas Propag. Mag.*, vol. 49, no. 6, pp. 24–39, Dec. 2007.

[5] J. Ma, R. Shrestha, L. Moeller, and D. M. Mittleman, "Invited article: Channel performance for indoor and outdoor terahertz wireless links," *APL Photon.*, vol. 3, no. 5, 2018, Art. no. 051601.

[6] R. Piesiewicz, M. Jacob, M. Koch, J. Schoebel, and T. Kurner, "Performance analysis of future multigigabit wireless communication systems at THz frequencies with highly directive antennas in realistic indoor environments," *IEEE J. Sel. Topics Quantum Electron.*, vol. 14, no. 2, pp. 421–430, Mar./Apr. 2008.

[7] S. Priebe and T. Kurner, "Stochastic modeling of THz indoor radio channels," *IEEE Trans. Wireless Commun.*, vol. 12, no. 9, pp. 4445–4455, Sep. 2013.

[8] D. Turchinovich, A. Kammoun, P. Knobloch, T. Dobbertin, and M. Koch, "Flexible all-plastic mirrors for the THz range," *Appl. Phys. A*, vol. 74, no. 2, pp. 291–293, 2002.

[9] M. Koch, "Terahertz communications: A 2020 vision," in *Terahertz Frequency Detection and Identification of Materials and Objects*. Berlin, Germany: Springer, 2007, pp. 325–338.

[10] T. Kürner, D. M. Mittleman, and T. Nagatsuma, *THz Communications: Paving the Way Towards Wireless Tbps*. Berlin, Germany: Springer, 2022.

[11] M. N. Islam and M. Koch, "Terahertz patch antenna arrays for indoor communications," in *Proc. Int. Conf. Next- Gener. Wireless Syst.*, 2006, Paper WC02-1.

[12] K.-I. Maki and C. Otani, "Terahertz beam steering and frequency tuning by using the spatial dispersion of ultrafast laser pulses," *Opt. Express*, vol. 16, no. 14, pp. 10158–10169, 2008.

[13] B. Scherger et al., "Discrete terahertz beam steering with an electrically controlled liquid crystal device," *J. Infrared, Millimeter, Terahertz Waves*, vol. 33, no. 11, pp. 1117–1122, 2012.

[14] Y. Monnai et al., "Terahertz beam steering and variable focusing using programmable diffraction gratings," *Opt. Express*, vol. 21, no. 2, pp. 2347–2354, 2013.
[15] X. Liu et al., "Terahertz beam steering concept based on a MEMS-reconfigurable reflection grating," *Sensors*, vol. 20, no. 10, 2020, Art. no. 2874.
[16] J. Wu et al., "Liquid crystal programmable metasurface for terahertz beam steering," *Appl. Phys. Lett.*, vol. 116, no. 13, 2020, Art. no. 131104.
[17] J. M. Seifert, G. G. Hernandez-Cardoso, M. Koch, and E. Castro-Camus, "Terahertz beam steering using active diffraction grating fabricated by 3D printing," *Opt. Express*, vol. 28, no. 15, pp. 21737–21744, 2020.
[18] R. Piesiewicz et al., "Terahertz characterisation of building materials," *Electron. Lett.*, vol. 41, no. 18, pp. 1002–1004, 2005.
[19] R. Piesiewicz et al., "Scattering analysis for the modeling of THz communication systems," *IEEE Trans. Antennas Propag.*, vol. 55, no. 11, pp. 3002–3009, Nov. 2007.
[20] C. Jansen et al., "Diffuse scattering from rough surfaces in THz communication channels," *IEEE Trans. Terahertz Sci. Technol.*, vol. 1, no. 2, pp. 462–472, Nov. 2011.
[21] M. Urahashi and A. Hirata, "Complex permittivity evaluation of building materials at 200-500 GHz using THz-TDS," in *Proc. Int. Symp. Antennas Propag.*, 2021, pp. 539–540.
[22] H.-J. Song and T. Nagatsuma, "Present and future of terahertz communications," *IEEE Trans. Terahertz Sci. Technol.*, vol. 1, no. 1, pp. 256–263, Sep. 2011.
[23] M. Jacob et al., "Diffraction in mm and sub-mm wave indoor propagation channels," *IEEE Trans. Microw. Theory Techn.*, vol. 60, no. 3, pp. 833–844, Mar. 2012.
[24] T. Schneider, A. Wiatrek, S. Preußler, M. Grigat, and R.-P. Braun, "Link budget analysis for terahertz fixed wireless links," *IEEE Trans. Terahertz Sci. Technol.*, vol. 2, no. 2, pp. 250–256, Mar. 2012.
[25] C. Han, A. O. Bicen, and I. F. Akyildiz, "Multi-ray channel modeling and wideband characterization for wireless communications in the terahertz band," *IEEE Trans. Wireless Commun.*, vol. 14, no. 5, pp. 2402–2412, May 2015.
[26] Z. Xu, X. Dong, and J. Bornemann, "Design of a reconfigurable MIMO system for THz communications based on graphene antennas," *IEEE Trans. Terahertz Sci. Technol.*, vol. 4, no. 5, pp. 609–617, Sep. 2014.
[27] K. Guan et al., "On millimeter wave and THz mobile radio channel for smart rail mobility," *IEEE Trans. Veh. Technol.*, vol. 66, no. 7, pp. 5658–5674, Jul. 2017.
[28] F. Sheikh, Q. H. Abbasi, and T. Kaiser, "On channels with composite rough surfaces at terahertz frequencies," in *Proc. IEEE 13th Eur. Conf. Antennas Propag.*, 2019, pp. 1–5.
[29] M. Wang et al., "Reflection characteristics measurements of indoor wireless link in D-band," *Sensors*, vol. 22, no. 18, 2022, Art. no. 6908.
[30] J. Ma, R. Shrestha, W. Zhang, L. Moeller, and D. M. Mittleman, "Terahertz wireless links using diffuse scattering from rough surfaces," *IEEE Trans. Terahertz Sci. Technol.*, vol. 9, no. 5, pp. 463–470, Sep. 2019.
[31] P. Beckmann and A. Spizzichino, "The Scattering of Electromagnetic Waves From Rough Surfaces. Norwood, MA, USA: Artech House, 1987.
[32] W. Withayachumnankul and M. Naftaly, "Fundamentals of measurement in terahertz time-domain spectroscopy," *J. Infrared, Millimeter, Terahertz Waves*, vol. 35, pp. 610–637, 2014.
[33] D. Didascalou, M. Dottling, N. Geng, and W. Wiesbeck, "An approach to include stochastic rough surface scattering into deterministic ray-optical wave propagation modeling," *IEEE Trans. Antennas Propag.*, vol. 51, no. 7, pp. 1508–1515, Jul. 2003.

Fatima Taleb received the B.Sc. and M.Sc. degrees in communications engineering from the University of Aleppo, Aleppo, Syria, in 2010 and 2016, respectively.

She worked from 2011 to 2014 as a Research Assistant with Communications Engineering Department, Faculty of Electrical and Electronic Engineering, University of Aleppo. Since 2018, she has been a Research Associate of experimental semiconductor physics with the University of Marburg, Marburg, Germany. Her current research focus on THz communication systems.

Goretti G. Hernandez-Cardoso was born in 1995 in Zacatecas, Mexico. She received the bachelor's degree in physics from the Universidad Autonoma de Zacatecas, Zacatecas, in 2014, and the master's and Ph.D. degrees in science (optics) from the Centro de Investigaciones en Optica, Leon, Mexico, in 2016 and 2020, respectively.

During her Ph.D. studies, she spent one year with Semiconductor Photonics Group, Marburg, Germany. She is currently a Postdoctoral Research Fellow with Physics Department, Philipps-Universität Marburg, Marburg, Germany.

Enrique Castro-Camus received the B.Sc. degree in physics from the Universidad Nacional Autonoma de Mexico, Mexico City, Mexico, in 2002, and the Dr. Phil. (Ph.D.) degree in condensed matter physics from the University of Oxford, Oxford, U.K., in 2006.

In 2009, he joined the Centro de Investigaciones en Optica, Mexico. In 2021, he was honored with a Guest Professorship with Philipps-Universitat Marburg, Germany. He has taken part as an Editor and an organizer of multiple scientific journals and events. His research interests include the applications and development of terahertz spectroscopy techniques with particular emphasis on the study of ultrafast charge transport in semiconductors, as well as exploring uses of THz radiation in multiple disciplines, such as biology, astronomy, conservation of objects with cultural value, medicine, and industry.

Dr. Castro-Camus was a recipient of the Young Scientist Award from IRMMW-THz Society and the Alexander von Humboldt Experienced Research Fellowship.

Martin Koch received the Diploma and Ph.D. degrees in physics from Philipps-Universität Marburg, Marburg, Germany, in 1991 and 1995, respectively.

He was a Postdoctoral Fellow with Bell Labs/Lucent Technologies, Holmdel, NJ, from 1995 to 1996. From 1996 to 1998, he was with Photonics and Optoelectronics Group, University of Munich, Munich, Germany. Since 1998, he has been an Associate Professor with the Department of Electrical Engineering, Technische Universität Braunschweig, Braunschweig, Germany. In 2003, he spent a three-month sabbatical with the University of California Santa Barbara, Santa Barbara. Since 2009, he has been a Professor of experimental semiconductor physics with Philipps-Universität Marburg.

Dr Koch was a recipient of the Kaiser–Friedrich Research Prize in 2003, the IPB Patent Award in 2009, and the Exceptional Service Award of the IRMMW-THz Society in 2019. He is the Editor-in-Chief for the *Journal of Infrared, Millimeter, and Terahertz Waves*.